Transformation to amorphous state of metals by ion implantation: P in Ni

C. Cohen
Groupe de Physique des Solides de l'Ecole Normale Supérieure, Université Paris VII, 75221 Paris, France

A. Benyagoub, H. Bernas, J. Chaumont, and L. Thomé
Centre de Spectrométrie Nucléaire et de Spectrométrie de Masse, Boîte Postale No. 1, 91406 Orsay, France

M. Berti and A. V. Drigo
Dipartimento di Fisica, Universita di Padova, Unita Gruppo Nazionale di Struttura della Materia, Padova, Italy
(Received 25 July 1984)

The amorphization of Ni single crystals by P ion implantation was studied via *in situ* Rutherford backscattering and channeling experiments. Both the P-implant and the Ni-disorder profiles were analyzed. At 90 K, no P mobility was found under implantation. The fluence dependence of the disorder level is analyzed in terms of amorphous-cluster formation above a threshold P concentration. The radius of the clusters is four interatomic distances, i.e., the correlation length of a typical amorphous lattice as determined in structure-sensitive experiments. The amorphous fraction α in the implanted layer is $\alpha=0.5$ when $x\sim0.12$ ($Ni_{1-x}P_x$) and $\alpha=1$ when $x\sim0.15$. At 300 K, short-range P motion occurs during implantation. Amorphous clusters are formed even at low P concentrations ($x\sim0.05$). The P-to-Ni ratio in the clusters is that of the eutectic, and we found $\alpha=1$ at the eutectic composition. There is evidence that the amorphization mechanism described in this paper also holds for other metal-metalloid systems.

I. INTRODUCTION

There has been a wealth of experimental and theoretical work on the structure and the formation of amorphous metallic alloys, much of it recently summarized.[1,2] The formation problem has been approached mainly from a thermodynamical viewpoint, e.g., by establishing formation and amorphous-phase stability criteria. Work on the construction of the amorphous lattice from appropriate elementary structures has been restricted essentially to computer modeling[3–5] or theoretical analysis,[6,7] although the advent of new cluster-physics techniques[8,9] raises hopes of direct experimental access.

In this paper we report channeling experiments on Ni crystals implanted with increasing phosphorus concentrations which provide rather direct information on the mechanism by which an amorphous metallic lattice is built up from an increasing number of elementary clusters. A simple statistical model accounts for the amorphization process at liquid-nitrogen temperature (LNT): the minimum radius of an amorphous cluster is found to be ~10 Å, i.e., the typical value of the amorphous-lattice correlation length deduced from structure-sensitive experiments performed on a-$Pd_{80}Si_{20}$,[10] a-$Fe_{80}B_{20}$,[11] a-$Ni_{82}B_{18}$, and a-$Ni_{66}B_{34}$.[12,13] A comparison of channeling experiments at LNT and room temperature (RT) shows that the buildup mechanism is basically identical, but reveals differences in the P-to-Ni number ratios in the amorphous clusters: The latter are discussed in terms of local phase stability criteria, which differ depending on thermodynamical equilibrium. Preliminary results were presented some time ago.[14]

A number of metallic glasses have been produced previously by ion implantation,[15–21] with the goal of comparing their characteristics (structure, electronic properties) to those of their counterparts produced by other techniques, or alternatively, of producing new glasses by forcing solubility limits. So far, these experiments have been discussed mainly in relation to thermodynamic-equilibrium phase diagrams[21] and, more recently, in relation to the effect of damage cascades on the crystal-to-amorphous phase transition.[22] From the latter point of view, ion-implantation experiments are complicated (except when self-implantation is performed), since the chemical composition and the structural order are changed simultaneously; defect mobility, where present, further complicates matters. Irradiation (rather than implantation) experiments are thus generally a more appropriate way of studying the driving force due to damage on the crystalline- or amorphous-structure stability criteria. As discussed below, this restriction does not apply to a study of the amorphization mechanisms.

Schematically, the situation here is as follows. We start from a pure single crystal of Ni, into which increasing amounts of P are implanted. Each incoming P ion, with an energy of ~100 keV, displaces some 10^3 target atoms. Many (or most, depending on the target temperature and hence defect mobility) of these defects recombine in very short times; dislocations are produced, in increasing numbers and size, as the fluence is increased, until a dense dislocation network pervades the implanted layer. Above P concentrations of a few atomic percent (see below), amorphization sets in, as shown by channeling, transmission-electron-microscopy[23] (TEM), and x-ray diffraction[24] experiments. The dislocation network seen in TEM is progressively washed out as amorphization

progresses. At high P concentration (above 15—20 at. %), the entire implanted layer is amorphous. It should be stressed that, by this time, each atom in the implanted layer has been displaced some 100 times, on the average. When analyzing the amorphization process, one cannot neglect the effect of these repeated displacements, particularly in discussing the stability of amorphous clusters.

II. EXPERIMENTAL DETAILS

The Ni single crystals used were oriented along the [100] direction. They were mechanically and then electrochemically polished. For one experiment (see Appendix) a 13-nm-thick C film was deposited on half of the crystal surface.

Implanted-P profiles were measured at different implantation fluences by using Ni thin films (about 200 nm thick) evaporated on a Be substrate in a vacuum better than 10^{-7} Torr.

Phosphorus implantation was performed at the Centre de Spectrométrie Nucléaire et de Spectrométrie de Masse (CSNSM) implanter in Orsay under a vacuum of $(2—5)\times10^{-8}$ Torr.[25] The energy was 125 keV, and the total fluence ranged from 5×10^{15} to 3×10^{17} P atoms cm^{-2}. A three-axis goniometer allowed alignment of the crystal, and the implantation was always performed in a random direction by tilting the crystal away from any major lattice direction. The substrate was held either at LNT or at RT depending on the experiment. The implantation dose rate was always kept below 1.5 $\mu A\,cm^{-2}$ in order to avoid sample heating. The temperature of the samples was monitored by a Pt resistor fixed inside the sample holder. The LNT was actually 88 K and rose to 95 K during implantation.

Channeling measurements were performed *in situ* after each implantation and at the implantation temperature by using a 380-keV $^4He^{2+}$ beam delivered by the CSNSM implanter itself. In order to check the effect of thermal vibrations on channeling and to compare LNT and RT experiments, channeling measurements were performed on samples implanted at LNT, both at LNT and at RT for several implantation fluences.

After a series of implantations and *in situ* measurements, channeling experiments were performed at RT by using the 2-MV Van de Graaff accelerator of both the Ecole Normale Supérieure (Paris) and the Laboratori Nazionali di Legnaro (Padova). In the high-energy experiments, the P-concentration profiles at the higher implanted fluences could be rather accurately deduced from the change in the Ni level of the random spectrum. The measurements were calibrated to an accuracy better than 2% (Ref. 26) by using absolute backscattering standards.[27] The depth resolution at all Rutherford-backscattering (RBS) energies was about 10 nm, i.e., much smaller than the implanted-ion range.

III. DATA REDUCTION

The channeling surface peak was obtained by following the procedure described by Stensgaard *et al.*[28] The surface peak of the unimplanted crystals was always found to be slightly higher than the theoretical value for a perfect and unoxidized crystal[28] by an amount corresponding to $(3.0\pm0.4)\times10^{15}$ Ni atoms cm^{-2}. The oxygen contamination of the samples was measured by using the $^{16}O(d,p)\,^{17}O^*$ nuclear-reaction[29] yield calibrated against absolute standards.[30] It was always found to match the excess Ni amount in the channeling surface peak very closely: We conclude that this excess is due to a surface oxide layer 1 to 2 monolayers thick. This result confirms the quality of our polishing technique.

Dechanneling curves were obtained by normalizing the channeling yield to the random yield at the same energy, i.e., neglecting any possible difference in the energy loss of the channeled and random beams.

The P-implantation profiles were deduced from the experimental RBS spectra obtained with a 1.8-MeV $^4He^+$ beam. A computer program developed at Padova[31] first calculates an approximate profile by comparing the signals corresponding to particles backscattered on Ni atoms for implanted and unimplanted samples. This comparison is performed at the same incident energy, taking into account the different energy loss of the incoming particles. The energy-to-depth conversion is calculated for the implanted sample by assuming that Bragg's additivity rule applies to the stopping powers. The profile obtained in this way is then used as a starting trial profile for a computed best fit of the overall spectrum, fitting both the Ni and P signals. The resulting profile depends, of course, on the stopping powers used. In our case the stopping powers were deduced directly from the thin-film spectra, after calibrating them against the absolute RBS standard, and were found to be about 5% and 10% lower than those reported by Ziegler[32] for Ni and P, respectively.

IV. RESULTS AND DISCUSSION

TEM (Ref. 23) and grazing incidence x-ray[24] experiments have given direct structural proof that, above a threshold fluence, P-implanted Ni is progressively amorphized; this result is also obtained indirectly from electrical-conductivity experiments.[33,34] In the following subsections, we first compare the P-implantation profiles to the implantation-induced disorder profiles in the Ni lattice, and we show that the latter are directly due to the former. We then analyze the P-implantation fluence dependence of the disorder.

A. Phosphorus-implantation profile

The thin Ni films were implanted both at RT and LNT at total fluences ranging from 2×10^{16} to 3×10^{17} P atoms cm^{-2}. The Ni contents measured by RBS before and after implantation led to an average sputtering coefficient $S=1.4$.

Consider (Fig. 1) the RBS spectrum recorded for a sample implanted with 2.4×10^{16} P atoms cm^{-2} at RT. The solid line represents the computer-generated spectrum obtained with the P profile (solid line) shown in the inset. This profile can be approximated by a Gaussian with a peak position at 59 nm below the surface and with a full width at half maximum (FWHM) of 78 nm. Sputtering broadens the original implantation distribution and shifts

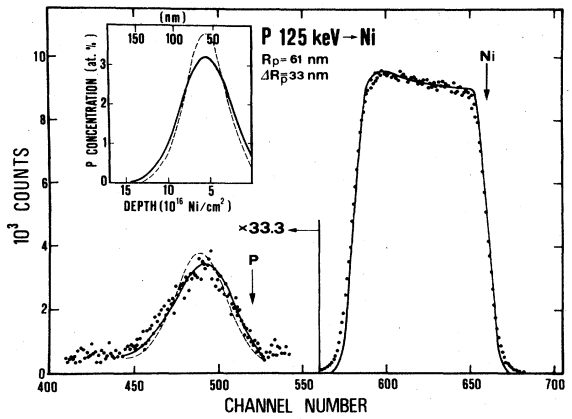

FIG. 1. RBS spectrum on a Ni film implanted at 125 keV (RT) with 2.4×10^{16} P atoms cm^{-2}. Analyzing particles, 1.8-MeV ^4He ions; energy calibration, 2.15 keV/channel. The solid line is a fit to the experimental spectrum using the P profile shown in the inset (solid line). The dashed line is a simulation using the profile (dashed line in the inset) calculated from the program TRIM. Note that on the Ni signal the difference between the two profiles is negligible.

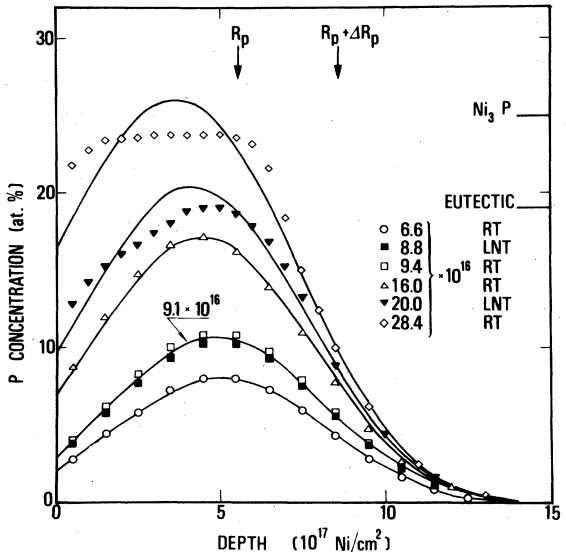

FIG. 2. Distribution profiles of P ions implanted at 125 keV in Ni films extracted from the fit of experimental RBS spectra. The solid lines are the calculated profiles obtained for each fluence using experimental values of R_p, ΔR_p, and S.

it towards the surface. In our case the sputtered-off layer was about 4 nm thick and had a negligible effect (within the experimental uncertainties) on the width of the distribution, whereas it caused a shift of about 2 nm in the peak position. We conclude that the original implantation profile of 125-keV P ions in Ni is characterized by the parameters $R_p=61$ nm and $\Delta R_p=33$ nm. These values are higher than the Winterbon-Sigmund-Sanders (WSS) values:[35] 53 and 24 nm, respectively. The dashed curves in Fig. 1 are the result of a calculation based on the program TRIM (Ref. 36) normalized to the total P fluence: The projected range (64 nm) is in good agreement with the experimental value, whereas the experimental profile width is about 20% larger than the calculated ΔR_p value (27.5 nm). The sensitivity of our fitting procedure[31] allows us to assert that the spectra calculated from WSS and TRIM do not fit the experimental profiles. A calculation of the ion-beam-mixing effect on the implantation profile was performed following the Sigmund-Gras-Marti[37] theory. The result shows that mixing had a negligible effect on the distribution width compared to the effect of sputtering, whatever the P fluence.

Phosphorus profiles for different implantation fluences at LNT and at RT were measured on thin films and similarly compared to the profiles calculated on the basis of our experimental implantation and sputtering parameters. The results are shown in Fig. 2. The thin films implanted at LNT were analyzed only after annealing at RT, owing to the need of a high-energy beam for the depth-profile analysis. However, P is not mobile in Ni at RT, so that the measured profiles are likely to correspond to the as-implanted profiles. We checked that, for a given fluence, they were identical to those of the corresponding RT-implanted samples, as shown in Fig. 2 for 9×10^{16} P atoms cm^{-2}. The procedure discussed above led to good agreement between the experimental and calculated profiles for implantation fluences lower than 2×10^{17} P atoms cm^{-2}. We conclude that for these fluences there is no long-range migration of P and, in particular, no preferential migration towards the surface.

The situation is markedly different for P-implantation profiles obtained at higher fluences, where profile broadening sets in. In fact, the profile was practically flat between the surface and $R_p+\Delta R_p$ at the highest fluence studied. The profile broadening cannot be accounted for by the change in sputtering efficiency due to the P concentration at the surface: The profile flattening was so large at a fluence of 2.8×10^{17} P atoms cm^{-2} that it implies P-atom mobility through out the region in which implantation damage is produced. As seen in Fig. 2, this effect occurs even at LNT.

Our concentration-profile measurements allow us to relate this effect to critical compositions of the Ni-P system (as found in the equilibrium phase diagram): The P-profile broadening—and corresponding defect-enhanced P mobility—sets in when the P concentration at R_p reaches 19 at. %, which is the deep eutectic composition. This intrusion of the equilibrium phase properties in both LNT and RT experiments on high-fluence implants is a point to be accounted for below. Radiation-induced mobility of P at concentrations in excess of 25 at. % has been already reported by us in a previous paper.[38] In the same paper, radiation-enhanced mobility of P was assumed to occur at RT, even at low concentrations, in order to explain the nearly flat depth profile observed at that time. This contradicts our present result; as discussed in the Appendix, the previous result was due to the low P-implantation energy (80 keV).

B. Channeling results

Aligned and random RBS spectra were registered *in situ* for crystals implanted at RT and LNT with in-

creasing ^{31}P fluences from 5×10^{15} up to 2.9×10^{17} atoms cm^{-2}. In every case, the surface-peak area (where measurable) remained small, as in the spectrum of Fig. 3(a), demonstrating that no enhanced disordering of the crystal surface [such as that due to recoil implantation of a contamination layer shown in Fig. 3(b)] occurred. Information about the disordering process was extracted from the analysis of the [110]-aligned backscattering yields as a function of depth at different P fluences. These yields, $\chi(t)$, normalized to the random yields, are presented in Figs. 4(a) (RT implants) and 4(b) (LNT implants). The results for the RT and LNT implants both showed strong dechanneling, with a broad peak appearing around $t=R_p$ when the implanted-P fluence rose above some (implantation-temperature-dependent) value. Moreover, this broad peak first reached the random yield ($\chi=1$) at R_p, and then broadened increasingly with the P fluence.

The presence of a maximum in the dechanneling curves is indicative of backscattering on Ni atoms randomly distributed with respect to the crystal lattice and localized at a given depth. If crystal distortions alone were present, they would only induce dechanneling and lead to a monotonous behavior in the $\chi(t)$ curves, as observed, e.g., for self-implanted metals.[39] A comparison of the dechanneling peaks to the P-implantation profiles (Sec. IV A) clearly demonstrates that the existence of Ni atoms in "random" sites is related to the presence of P atoms.

Channeling alone cannot discriminate whether these Ni atoms are associated to P in amorphous clusters or in randomly oriented polycrystalline phases. Other experiments demonstrated that amorphization does indeed take place. X-ray-diffraction analyses[24] were performed on our crystals after P implantation at fluences for which $\chi(t)=1$ between the surface and $R_p+\Delta R_p$, and they revealed that the alloys were totally amorphous. Similar results were also found in TEM (Ref. 23) and resistivity (Refs. 33 and 34) experiments performed on Ni polycrystalline thin films implanted at the same P concentration at 6—10 K and RT. We conclude that the maximum observed in the

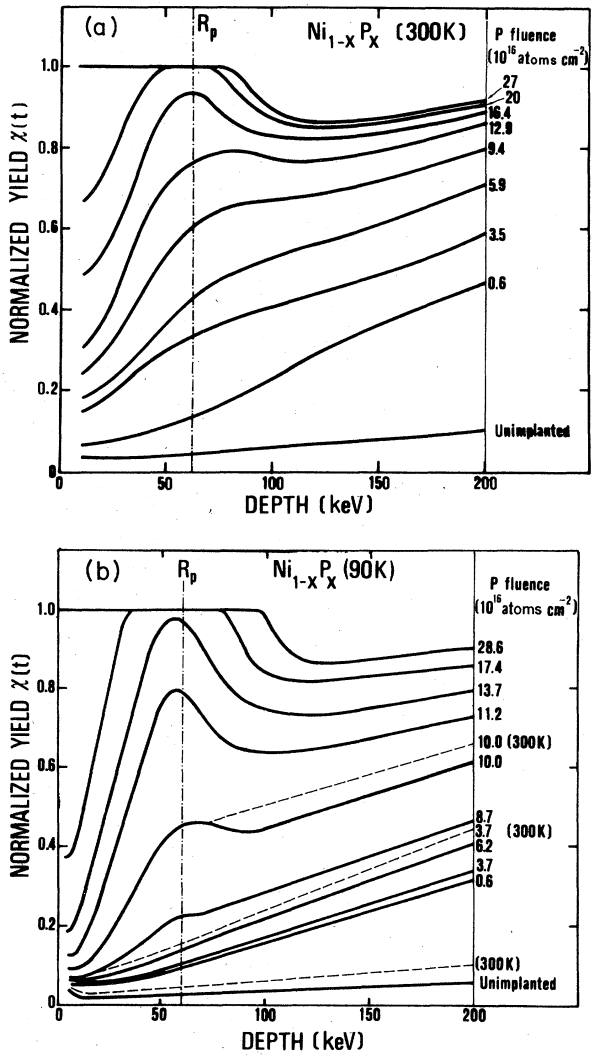

FIG. 4. Depth dependence of the [100]-aligned RBS yields normalized to the random yields for P-implanted Ni single crystal at (a) RT and (b) LNT. Phosphorus-ion-implantation energy, 125 keV; analyzing particles, 380-keV ^4He ions.

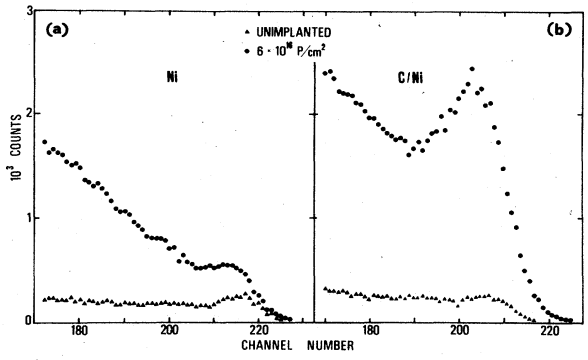

FIG. 3. [100]-aligned RBS spectra recorded on a Ni single crystal after implantation of 6×10^{16} P atoms cm^{-2} at RT. (a) Electropolished crystal surface; (b) same with a 13-nm-thick carbon layer deposited on the surface of the crystal before implantation. Analyzing particles, 380-keV ^4He ions; energy calibration, 1.3 keV/channel.

$\chi(t)$ curves in the channeling experiments is *due to the presence of amorphous clusters* and that its study provides information about the amorphization mechanism.

This information is obtained from a comparison of the $\chi(t)$ curves with the implantation profiles presented in Sec. IV A. The peak in $\chi(t)$ at R_p reaches the random level and begins to broaden for P fluences at which the profiles of Fig. 2 display P mobility towards the surface. We conclude that, when a continuous amorphous layer is formed at a given depth, additional P atoms implanted in this region are mobile under irradiation and diffuse towards the boundaries of the amorphous layer, leading to growth of the amorphous phase. This process takes place during both RT and LNT implants: it only occurs in the presence of implantation-induced mobility, as evidenced by the absence of any change in the P-implant and Ni-disorder profiles when a LNT-implanted sample is annealed up to RT (Sec. IV C). In addition, we find that

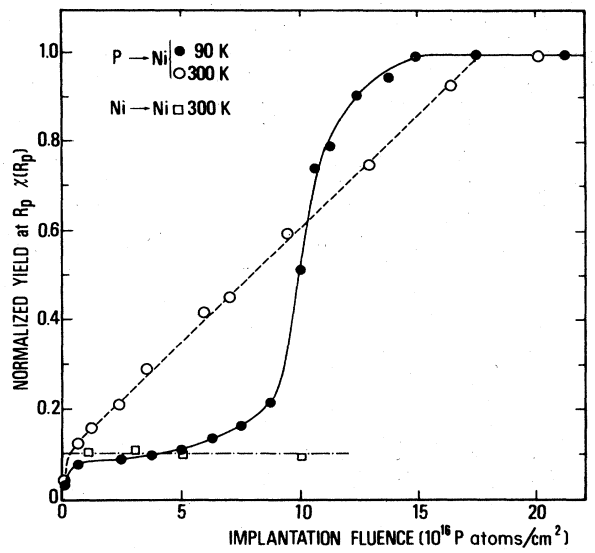

FIG. 5. Aligned RBS yields at R_p (normalized to random yields) versus implantation fluence. Phosphorus implanted into Ni at LNT (solid circles) and RT (open circles), and RT self-implanted Ni (open squares).

phosphorus migration only occurs into regions where the implantation-induced damage level is quite high (e.g., the amorphous region extends only down to $t \sim R_p + \Delta R_p$ at our highest implanted fluences).

There are also striking differences in the disordering process for RT and LNT implants, as shown in Fig. 5, in which we have plotted the normalized channeling yield at depth R_p (i.e., where the P concentration can be considered to be constant within 3% in a depth window corresponding to our experimental resolution, ~ 100 Å) deduced from Figs. 4(a) and 4(b). Besides the obvious difference in the slopes of the curves and the appearance of a threshold effect in the LNT experiments, the fact that $\chi(R_p)$ reaches the random level for markedly lower fluences at LNT than at RT must also be accounted for.

Figure 5 also shows the values of $\chi(R_p)$ obtained for self-implantation of Ni at 190 keV, this energy being chosen in order to correspond to the same R_p value as that of 125-keV P ions. When Ni is implanted, $\chi(R_p)$ saturates at values around 0.1. The stabilization of disorder by P atoms is obvious.

C. Disorder analysis and evaluation

In order to study the amorphization process, the amorphous fraction α at R_p must be related to the measured $\chi(R_p)$. Our analysis is based on the following assumption: Above some implanted P fluence, the implanted layer contains both amorphous and crystalline zones; we write the total aligned yield χ as a sum of the contributions due to the crystalline and amorphous zones. Except at the lowest fluences, it is reasonable to expect that these contributions are, in fact, correlated, i.e., that the yield from the crystalline zones depends on the fraction of amorphous material. This was demonstrated by recording channeling spectra with ^{4}He ions at different energies between 400 keV and 1.8 MeV on samples implanted at RT and LNT up to fluences such that $\chi(R_p) \sim 0.5$. For these measurements, the LNT-implanted sample had to be warmed to RT and analyzed with a 2-MeV ^{4}He beam. We have already shown in Sec. IV A that this treatment does not induce any P-profile modification, and, in Sec. IV B, it was shown that no change is observed in the disorder profile. In fact, as shown in Fig. 4(b), small differences are obtained in $\chi(t)$, after annealing at RT, a crystal implanted at LNT with P fluences up to 4×10^{16} atoms cm^{-2}. This is due to an increase of dechanneling induced by larger thermal vibrations. For higher fluences, however, disorder dominates the dechanneling process and RT annealing has no effect on the dechanneling in the disordered region [see Fig. 4(b), 10^{17} P atoms cm^{-2}]. The values $\chi(t)$ obtained for various ^{4}He energies are displayed in Fig. 6. For RT- and LNT-implanted samples, nearly no probing-beam-energy dependence is observed in $\chi(t)$, whereas if dechanneling could be attributed independently to multiple scattering in the amorphous zones (fraction α), and to distortion of the remaining crystal lattice, the first contribution should dominate at 400 keV ($E^{-1/2}$ variation), and the second, at 1.8 MeV ($E^{1/2}$ variation). As a matter of fact, the value $\chi(R_p + \Delta R_p)$ is so high at 400 keV that this would imply a very large amorphous fraction α, whose direct contribution to $\chi(R_p)$ should be much higher than experimentally observed (the maximum at R_p is not very pronounced for these P fluences). We must then drop the assumption that the crystalline and amorphous contributions to dechanneling are independent. A more likely explanation involves the heterogene-

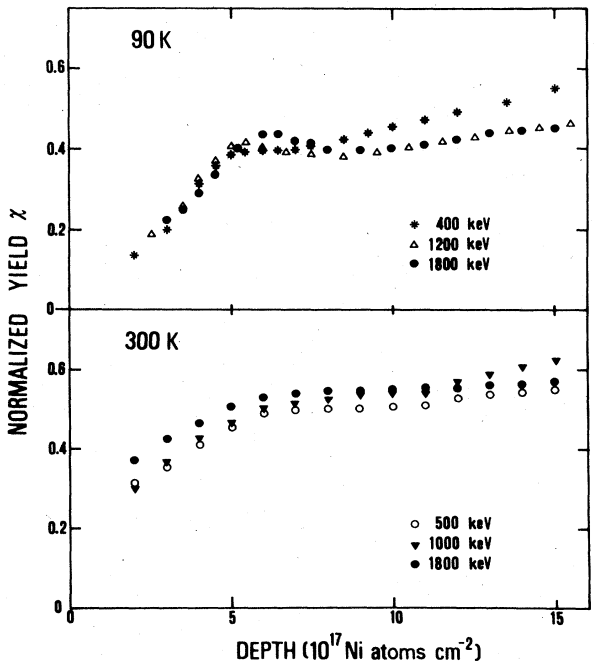

FIG. 6. Depth dependence of the [100]-aligned RBS yields (normalized to random yields) for LNT and RT P-implanted Ni using analyzing ^{4}He beams of different energies. At LNT the implantation fluence was 10^{17} P atoms cm^{-2}, whereas it was 5.9×10^{16} P atoms cm^{-2} at RT.

ous nature of the implanted layer. The crystalline lattice must accommodate the small amorphous clusters: This leads to interfaces in which considerable lattice distortion occurs, so that an initially aligned ^{4}He particle suffers a dechanneling process somewhat similar to that induced by stacking faults, i.e., probing-beam-energy independent.

In order to obtain the amorphous fraction $\alpha(R_p)$, we must assume that the backscattering yield in the crystalline fraction χ_c also depends on α. We can then write the total yield at depth R_p as

$$\chi=(1-\alpha)\chi_c(\alpha)+\alpha \ . \tag{1}$$

For the sake of simplicity, we have assumed a linear law for $\chi_c(\alpha)$:

$$\chi_c(\alpha)=\chi_c(0)+\alpha[\chi_c(1)-\chi_c(0)] \ . \tag{2}$$

The values $\chi_c(0)$ and $\chi_c(1)$ were obtained at R_p by linear interpolation between the surface yield and the yield at $R_p+\Delta R_p$, as schematically illustrated in Fig. 7(a). The value $\chi_c(0)$ is taken at an implantation fluence for which a maximum of $\chi(t)$ at R_p just begins to appear, and $\chi_c(1)$ is associated with the fluence at which $\chi(R_p)$ just reaches the random level. Introducing the value $\chi_c(\alpha)$ given by (2) in Eq. (1) leads to a relation between α and χ. The values of α at R_p can then be determined from the values of χ at R_p reported in Fig. 5. Conversely, when α is determined, the function $\chi_c(\alpha)$ in Eq. (2) is known.

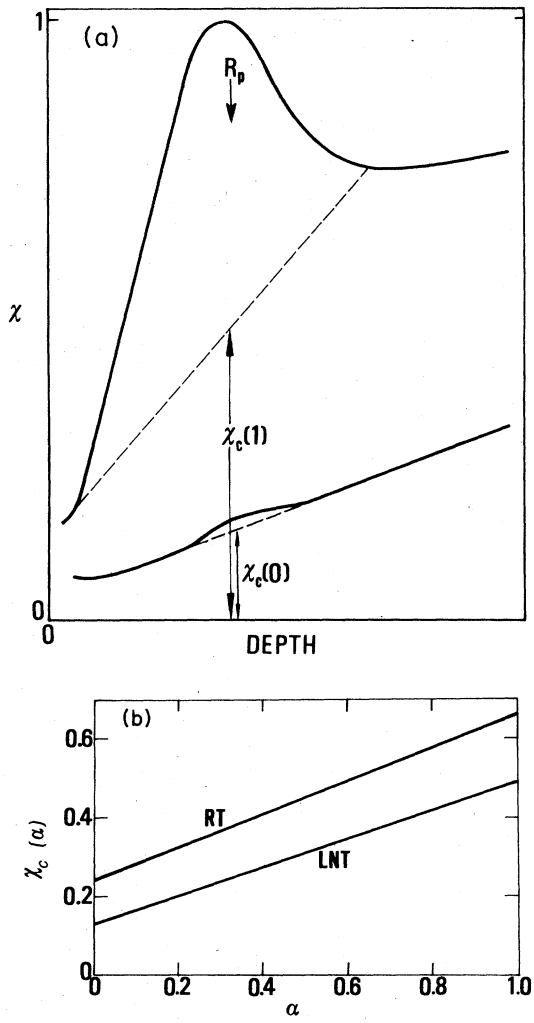

FIG. 7. (a) Schematic illustration of the procedure used to determine the quantities $\chi_c(0)$ and $\chi_c(1)$ in Eq. (2) from [100]-aligned RBS yields of Fig. 4 (for discussion, see Sec. IV C); (b) functions $\chi_c(\alpha)$ versus α for RT and LNT implants.

The functions $\chi_c(\alpha)$ were obtained in this way both for LNT and RT experiments. They are shown in Fig. 7(b). The two lines are nearly parallel and differ only in the values of $\chi_c(0)$. It must be pointed out that $\chi_c(0)$ corresponds to the yield measured at R_p in crystals already perturbed by P implantation, but at fluences for which amorphization has not set in. The values $\chi_c(0)$ are hence related to dechanneling induced both by thermal vibrations and by the extended defects produced by implantation. The differences in $\chi_c(0)$ for RT and LNT implants are too high to be accounted for only by differences in thermal vibrations; they are indicative of differences in the nature and number of extended defects, in good agreement with TEM results.[23] The significant feature for the present discussion is the fact that the slope of $\chi_c(\alpha)$ is nearly independent of implantation temperature. This slope is related to the dechanneling induced by consecutive crossing of amorphous clusters. Our result then shows that the "dechanneling efficiency" of the amorphous clusters does not depend on implantation temperature. This is a good indication that for a given amorphous fraction α, the probing beam crosses a mean number of amorphous clusters which does not depend on T: Although the details of the amorphization process are different at RT and LNT, the average size of the amorphous clusters formed is T independent. We shall relate this result to the structural properties of amorphous systems.

D. Amorphization mechanism

The variation of α at R_p as a function of the local P concentration is shown in Fig. 8 for RT and LNT experiments. It displays the same overall features as $\chi(R_p)$ in Fig. 5: a fairly slow-rising curve starting at very low P concentrations for RT implants, and a rather sharp transition above a concentration threshold for LNT implants. Full amorphization is reached at RT for a P concentration of 19 at. %, which corresponds exactly to the deep eutectic in the Ni-P phase diagram, while α is already unity for a P concentration of $\sim$15 at. % at LNT. This result is in agreement with the resistivity measurements of Refs. 33 and 34.

We first discuss the LNT results in terms of the simple assumption made in Sec. IV C, viz., that P implantation leads to the formation of amorphous clusters and that these clusters are amorphous because they contain a minimum amount of P atoms. (The following discussion applies only to implanted-P fluences such that no P mobility occurs.) In other words, the P atoms—if in sufficient number—stabilize the glass structure relative to the crystalline structure, in a situation where the high-energy-density cascades (and related atomic displace-

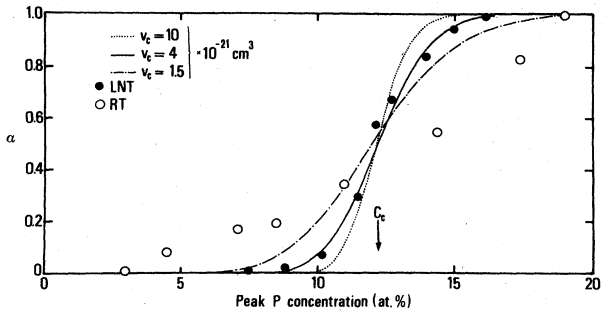

FIG. 8. P-concentration dependence of the amorphous fraction α for LNT (solid circles) and RT (open circles) implants. The solid line represents the best fit to the LNT experimental data using Eq. (4). Dashed lines are calculated, using Eq. (4), with different elementary volumes v_c of the amorphous clusters (see text).

ments) due to the incoming P ions constantly shake up the implanted lattice. Thus, although the system as a whole is far from equilibrium, the statistical energy-deposition mechanism allows it to minimize its energy locally, leading to a crystalline or glassy structure depending on the local P concentration.

The shape of the transition provides information on the minimal size v_c of the amorphous clusters formed. We assume that amorphization occurs when the number of P atoms in such a cluster is at least N_c. We subdivide the crystal around depth R_p into small identical volumes v_c. At a given implantation fluence, the mean number of P atoms in a volume v_c is $\overline{N}$, and the probability distribution of N around $\overline{N}$ is given by Poisson statistics:

$$P(N)=(\overline{N})^N \exp(-\overline{N})/N! \tag{3}$$

The amorphous fraction α for any average P concentration is given by the proportion of elementary volumes v_c for which $N \geq N_c$:

$$\alpha = \sum_{N=N_c}^{\infty} (\overline{N})^N \exp(-\overline{N})/N! \tag{4}$$

When N_c is sufficiently large, α is simply an error function.

The mean number $\overline{N}$ of P atoms in a cluster is directly proportional to the elementary volume v_c and to the mean concentration c of P in the sample. Labeling c_c the critical average concentration corresponding to N_c, the experimental curve α at LNT was fitted using Eq. (4) by varying the parameters c_c and v_c (see Fig. 8). The value of the parameters c_c and v_c is influenced, respectively, by the the position of the transition and the shape of the curve.

The best fit corresponds to the following values: $c_c = 12.2$ at. % and $v_c = 4 \times 10^{-21}$ cm^3, i.e., a sphere with a radius of four interatomic distances. Such a cluster contains about 400 atoms. The determination of the amorphous-cluster radius is rather precise. For example, Fig. 8 also shows calculated fractions α, using Eq. (4), with amorphous clusters whose radii correspond, respectively, to three and five interatomic distances: they clearly do not fit the results.

For RT implants, our channeling results show that amorphization already occurs when the mean P concentration is 3 times smaller than that at LNT (see Fig. 8). Attempts to fit the RT concentration dependence of α with Eq. (4) led to a meaningless result: the corresponding volume v_c has a "size" of about one interatomic distance. Moreover, the dechanneling analysis of Sec. IV C showed that the clusters must all have the same average size. The basic idea of amorphous-cluster formation—with a critical size—may still be retained under one further condition. As noted above, total amorphization occurs at RT when the overall average concentration corresponds to the thermodynamically favored, deep eutectic composition (19 at. % P). The simplest assumption is that as soon as the *average* P concentration has reached some 5 at. %, amorphous clusters may form with a uniquely defined composition—that of the eutectic—which is the nearest most-stable available amorphous phase. This clearly requires some P motion. This is in apparent contradiction with Sec. IV A, where we showed that long-range P migration is excluded below a P concentration of 19 at. %, but the formation of small clusters with a Ni-to-P ratio corresponding to the eutectic composition in a system whose average P concentration is 5 at. % only requires very-short-range rearrangements (a few interatomic distances on average). Such lattice rearrangements are quite conceivable, again assuming local minimization of the alloy's energy under implantation. At RT thermal energy provides an additional driving force for the crystalline-to-amorphous transition. Thus the amorphous fraction at RT should simply be proportional to the implanted-P concentration, in reasonable agreement with the results of Fig. 8.

In situ TEM studies of Ni-P and Pd-Si amorphization[23] agree with the results presented here and indicate an effect of implantation-induced dislocations on the buildup of the amorphous layer.

The situation is quite different when the P concentration is higher than ~ 19 at. %, i.e., when full amorphization occurs and long-range P diffusion takes place. This was previously studied[38] and is outside the scope of the present paper, although implantation-induced P mobility in the amorphous Ni-P system has implications on the stability of the latter.

E. Relation of the amorphization process to the metallic glass structure

In Sec. IV D the amorphization process was analyzed in statistical terms without any reference to the nature of the order (disorder) on a short-range scale. The analysis of the LNT experiments led us to introduce a characteristic size in our calculation: that corresponding to the radius (~ 10 Å) of the elementary amorphous cluster. It is noteworthy that such a characteristic length is also found in structural studies of metallic glasses. This was not true of early models[3–5] of the glass structure, but more realistic models[6,7] which take chemical short-range order (and the corresponding relation of the amorphous structure to that of its crystalline counterpart formed in the same

composition range) into account do find that the structural correlation in the glass extends over distances ~ 3—4 interatomic distances. The most recent stereochemical models (e.g., Refs. 7 and 40) lead to the concept of the glass as deduced from the corresponding crystal structure by a series of structural operations (such as twinning) with a correlation length determined by the basic features of short-range order, i.e., coordination number and range of the pair-correlation functions. Direct evidence for a correlation length of ~ 10 Å is provided by the coherent images obtained in high-resolution TEM experiments on a-$Pd_{80}Si_{20}$,[10] by the oscillations seen in the B pair-correlation functions for a-$Ni_{82}B_{18}$ and a-$Ni_{66}B_{34}$,[12,13] as well as by the range of oscillations in extended x-ray-absorption fine-structure experiments on, e.g., a-$Ni_{80}P_{20}$ (Ref. 41) or a-Ni_2B (Ref. 13). Nuclear-magnetic-resonance experiments[42] can also be interpreted in this way.

All these results point to this ~ 10 Å correlation length as the *maximum* distance over which short-range order can be defined in a glass (at least for metal-metalloid glasses). The results obtained in Sec. IV D strongly suggest that this correlation length is also the minimum distance over which the amorphous structure can be stablized in a crystalline lattice.

V. CONCLUSIONS

Ion implantation serves a double purpose in these experiments. The first is its capacity as a means of modifying the alloy composition in a controlled way. The second is related to the disorder accompanying the compositional change, but its action is less clear. Stable disordering due to simple displacement-cascade-damage overlap has been proven in semiconductors, but with the exception of Ga (Ref. 22) amorphization by damage cascades alone is certainly not evidenced in pure metals even at low temperatures,[43,44] where damage mobility and recombination are significantly reduced; attempts to relate disorder changes in metals to such implantation parameters as the deposited-energy density have only met with very limited success,[45] restricted to cases where the damage density was very low, and due to nonoverlapping cascades; implantation-induced amorphization of metals has so far only been found in cases where the disorder was produced by significant quantities of chemically active solute atoms.[14–21,46,47] One of the original purposes of the present work was to determine whether low-temperature implantation of metalloids could stabilize the glassy structure versus its crystalline counterpart at lower metalloid-atom concentrations than those necessary when preparing such amorphous systems by room-temperature implantation, or by the more familiar fast-quenching, sputtering, or chemical techniques. Our results do show that this is possible, but the reduction in amorphization threshold is only ~ 3 at. %, a significant increment, but not sufficiently large to invoke a drastic effect of radiation-damage stabilization. We conclude, in agreement with the now generally accepted view of glassy metals, that the chemical short-range order due to the solute atoms is the decisive factor in stabilizing lattice disorder. The repetitious role of the damage cascades is to randomly upset the geometry of the implanted layer, allowing any elementary assembly of atoms to choose its equilibrium configuration out of a moving spread of geometrical and compositional fluctuations.

Our results show that the spatial extent over which the implanted alloy minimizes its internal energy depends on the implantation fluence (via composition) and temperature. In the LNT experiments the energy minimization occurs via the formation of amorphous clusters—whose size is just the minimum size over which the amorphous structure may be defined—as soon as a threshold phosphorus concentration is reached. The stability of the amorphous component increases with the average P concentration as the eutectic concentration is approached. The average composition for which half of the sample has reached the amorphous state is just the bond-percolation threshold ($c_c = 0.12$) for the fcc lattice, a result that certainly requires further investigation.

In the RT experiments, the entire sample is amorphous only when the average composition has reached the eutectic composition (~ 19 at. %). It appears that the additional thermal energy is sufficient to enhance the scale over which minimization of the internal energy can occur: Lattice rearrangement (accompanied by short-range P motion) takes place under irradiation, and, consequently, only the most stable amorphous clusters are now formed at a P-to-Ni ratio corresponding to the eutectic composition.

We find that, at higher average P concentrations in Ni, P diffusion occurs under implantation (i.e., radiation induced) over the volume in which damage mobility occurs; clearly, as the temperature is raised, the scale over which energy minimization occurs increases and reaches the entire sample volume, so that the stability criteria for the glassy structure will just be those obtained at thermodynamical equilibrium.

Such internal-energy considerations can be extended in several ways. The first and most obvious regards the *irradiation-induced* amorphous-to-crystalline transition in a Ni-P system of constant composition: this transition should be concentration and temperature dependent. Experiments are underway to test this point. Secondly, the amorphization mechanism described in Sec. IV D should be operative at least in other metal-metalloid systems. This was demonstrated for the Pd-Si and Ni-B alloys, which we have studied at LNT and RT.[46,48] Preliminary results obtained at RT for the implanted Ta-B and Ta-P alloys show similar behavior,[47] as do the Nb-metalloid amorphization experiments of Linker.[20] It will be interesting to study the case of metal-metal systems. Finally, such local internal-energy fluctuations can also drive the heterogeneous nucleation of different crystalline phases in a given implanted crystalline alloy.

ACKNOWLEDGMENTS

We wish to thank K. Królas for his participation in the early stages of these experiments. The assistance of F.

Lalu, M. Salomé, and A. Rampazzo is also gratefully acknowledged. This work was supported by the Centre National de la Recherche Scientifique under Grant No. RCP-157 and by the Centre Nacional Recherche, Italy, under Grant No. 83.00025.02.

APPENDIX

In our previous work[38] the experimental profiles were compared to the WSS calculations, and at that time we did not know that the experimental ΔR_p is about 40% higher than the WSS value. As the implantations in Ref. 38 were performed at only 80 keV (i.e., $R_p = 40$ nm), even without any assumption of P mobility the profiles should be relatively flat from the surface inwards owing to the high ΔR_p value. The experimental results of Ref. 38 are, hence, consistent with the present ones, but our previous interpretation in terms of P mobility at RT has proven to be incorrect.

The absence of any difference between the RT and LNT P depth profiles is relevant to the interpretation of the experiment reported in Ref. 14. There, a linear fluence dependence of the surface channeling peak following phosphorus RT implantation was reported, in marked contrast to the LNT results. The difference was interpreted in terms of radiation-enhanced diffusion of P towards the surface, followed by the formation of amorphous clusters at the eutectic concentration. We have shown that there is no long-range P migration. Moreover, we were unable to reproduce this experiment under the same nominal conditions. However, a similar behavior was reported by Follstaedt *et al.*[49] in the case of Ti-implanted Fe and by Atkinson *et al.*[50] in the case of Fe-implanted Ti. In both cases the surface amorphization was attributed to C contamination of the sample surface.

In order to check this possibility, a 13-nm-thick C layer was deposited on half of the surface of a Ni single crystal. Phosphorus was then implanted at R_p over the entire crystal surface. The channeling spectra recorded on the two halves after each implantation fluence are completely different, as can be seen in Fig. 3 for 6×10^{16} P atoms cm^{-2}. The C-contaminated crystal exactly reproduces the results of Ref. 14, whereas the results for the clean crystal are identical to those reported for RT implantation in Sec. IV B. We conclude that the RT results of Ref. 14 were due to an erratic carbon contamination related to a faulty operation of the implantation-chamber vacuum system.

[1]*Glassy Metals,* Vol. 46 of *Topics in Applied Physics,* edited by H. J. Güntherodt and H. Beck (Springer, Berlin, 1981).

[2]Proceedings of the International Conference on Liquid and Amorphous Metals V, Los Angeles [J. Non-Cryst. Solids **61**, 1 (1984)].

[3]J. D. Bernal, Nature (London) **188**, 910 (1960); Proc. R. Soc. London, Ser. A **284**, 299 (1964).

[4]C. H. Bennett, J. Appl. Phys. **43**, 2727 (1972); T. Ichikawa, Phys. Status Solidi A **29**, 293 (1975); J. L. Finney, Mater. Sci. Eng. **23**, 199 (1976).

[5]D. S. Boudreaux and J. M. Gregord, J. Appl. Phys. **48**, 152 (1977); *ibid.* **48**, 5057 (1977); D. S. Boudreaux and H. J. Frost, Phys. Rev. B **23**, 1506 (1981).

[6]J. F. Sadoc, J. Dixmier, and A. Guinier, J. Non-Cryst. Solids **46**, 12 (1973); J. F. Sadoc and R. Mosseri, Philos. Mag. B **45**, 467 (1982).

[7]P. H. Gaskell, Nature (London) **276**, 484 (1978); J. Non-Cryst. Solids **32**, 207 (1979); in *Proceedings of the International Conference on Rapidly Quenched Metals, Sendai, 1981,* edited by T. Masumoto and K. Suzuki (The Metals Society, Sendai, Japan, 1982), p. 247.

[8]Proceedings of the International Conference on Small Particles and Inorganic Clusters, Lausanne [Surf. Sci. **106** (1981)].

[9]B. Mühlschlegel, in *International Advanced Course on Percolation, Localization and Superconductivity, NATO Advanced Science Institutes Series, Les Arcs, 1983,* edited by A. M. Goldman and S. A. Wolf (Plenum, New York, 1984), p. 65.

[10]P. H. Gaskell, L. A. Freeman, and D. J. Smith, in *Proceedings of the International Conference on Rapidly Quenched Metals, Sendai, 1981,* Ref. 7, p. 421.

[11]E. Nold, S. Steeb, P. Lamparter, and G. Rainer-Harbach, J. Phys. (Paris) Colloq. **41**, C8-186 (1980).

[12]G. S. Chadha, N. Cowlam, H. A. Davies, and I. W. Donald, J. Non-Cryst. Solids **44**, 265 (1981).

[13]J. Wong and H. H. Liebermann, Phys. Rev. B **29**, 651 (1984).

[14]C. Cohen, A. V. Drigo, H. Bernas, J. Chaumont, K. Królas, and L. Thomé, Phys. Rev. Lett. **48**, 1193 (1982).

[15]R. Andrew, W. A. Grant, P. J. Grundy, J. S. Williams, and L. T. Chadderton, Nature (London) **262**, 380 (1976).

[16]A. Ali, W. A. Grant, and P. J. Grundy, Philos. Mag. B **37**, 353 (1978).

[17]H. Bernas, A. Traverse, F. C. Zawislak, J. Chaumont, and L. Dumoulin, J. Phys. (Paris) Colloq. **41**, C8-859 (1980).

[18]L. Thomé, L. Mendoza-Zélis, L. Brossard, K. Królas, C. Cohen, J. Chaumont, and H. Bernas, Nucl. Instrum. Methods **199**, 437 (1982).

[19]B. Rauschenbach and K. Hohmuth, Phys. Status Solidi A **72**, 667 (1982).

[20]G. Linker, Nucl. Instrum. Methods **209-210**, 969 (1983).

[21]S. S. Lau, B. X. Liu, and M. A. Nicolet, Nucl. Instrum. Methods **209-210**, 97 (1983); B. X. Liu, W. L. Johnson, M. A. Nicolet, and S. S. Lau, *ibid.* **209-210**, 229 (1983).

[22]U. Göerlach, P. Ziemann, and W. Buckel, Nucl. Instrum. Methods **209-210**, 235 (1983).

[23]M. Schack, M. O. Ruault, and H. Bernas (unpublished).

[24]J. C. Pivin, C. Roques-Carmes, and J. Takadoum (unpublished).

[25]J. Chaumont, F. Lalu, M. Salomé, A. M. Lamoise, and H. Bernas, Nucl. Instrum. Methods **189**, 193 (1981).

[26]C. Cohen, J. A. Davies, A. V. Drigo, and T. E. Jackman, Nucl. Instrum. Methods **218**, 147 (1983).

[27]S. Rigo, C. Cohen, A. L'Hoir, and E. Backelandt, Nucl. Instrum. Methods **149**, 713 (1978).

[28]I. Stensgaard, L. C. Feldman, and P. J. Silverman, Surf. Sci. **77**, 513 (1978).

[29]G. Amsel and D. David, Rev. Phys. Appl. **4**, 383 (1969).

[30]G. Amsel, J. P. Nadai, C. Ortega, S. Rigo, and J. Siejka, Nucl. Instrum. Methods **149**, 705 (1978).

[31]M. Berti and A. Carnera (unpublished).

[32]J. F. Ziegler, *Stopping and Ranges of Ions in Matter* (Per-

gamon, New York, 1977), Vol. 4 (He).
[33]L. Mendoza-Zélis, L. Thomé, L. Brossard, J. Chaumont, K. Królas, and H. Bernas, Phys. Rev. B **26**, 1306 (1982).
[34]L. Thomé, A. Traverse, and H. Bernas, Phys. Rev. B **28**, 6523 (1983).
[35]K. B. Winterbon, *Ion Implantation Range and Energy Deposition Distributions* (Plenum, New York, 1975), Vol. 2.
[36]J. P. Biersack and L. G. Haggmark, Nucl. Instrum. Methods **174**, 257 (1980).
[37]P. Sigmund and A. Gras-Marti, Nucl. Instrum. Methods **168**, 389 (1980).
[38]L. Thomé, J. Chaumont, A. Traverse, H. Bernas, C. Cohen, M. Berti, and A. V. Drigo, Nucl. Instrum. Methods **209-210**, 1035 (1983).
[39]P. P. Pronko and K. L. Merkle, in *Applications of Ion Beams to Metals,* edited by S. T. Picraux, E. P. EerNisse, and F. L. Vook (Plenum, New York, 1974), p. 481.
[40]J. M. Dubois and G. Le Caer, J. Phys. (Paris) Colloq. **43**, C9-17 (1982).
[41]P. Lagarde, J. Rivory, and G. Vlaic, J. Non-Cryst. Solids **57**, 275 (1983).
[42]P. Panissod, I. Bakonyi, and R. Hasegawa, Phys. Rev. B **28**, 2374 (1983).
[43]A. Traverse, A. M. Lamoise, H. Bernas, and J. Chaumont, for Al-implanted Al, Ni-implanted Ni, and Ar-irradiated Pd, at 6 K (unpublished).
[44]B. Stritzker and J. Becker, Phys. Lett. **51A**, 147 (1975); O. Meyer, in *Application of Ion Beams to Materials,* edited by G. Cantor, J. S. Colligon, and W. A. Grant (Institute of Physics, Bristol, 1976), p. 168.
[45]For a review, see D. A. Thompson, Radiat. Eff. **56**, 105 (1981).
[46]X. J. Fan, A. Traverse, L. Thomé, A. Benyagoub, J. Chaumont, and H. Bernas, Radiat. Eff. **81**, 101 (1984).
[47]L. Thomé, J. C. Pivin, A. Benyagoub, H. Bernas, and R. W. Cahn, Ann. Chim. Fr. **9**, 287 (1984).
[48]L. Thomé, A. Benyagoub, C. Cohen, A. V. Drigo, M. Berti, and H. Bernas (unpublished).
[49]D. M. Follstaedt, J. A. Knapp, and S. T. Picraux, Appl. Phys. Lett. **37**, 330 (1980).
[50]R. Atkinson, G. Longworth, and R. E. J. Watkins, Radiat. Eff. **70**, 107 (1983).